

What Drives Daily Precipitation Over Central Amazon? Differences Observed Between Wet and Dry Seasons

T. S. Biscaro¹, L. A. T. Machado¹, and S. E. Giangrande²

¹Center for Weather Forecast and Climate Studies, National Institute for Space Research, Cachoeira Paulista, São Paulo, 12630000, Brazil.

²Environmental and Climate Sciences Department, Brookhaven National Laboratory, Upton, NY, USA.

Correspondence to: Thiago S. Biscaro (thiago.biscaro@inpe.br)

Abstract. Please use only the styles of this template (MS title, Authors, Affiliations, Correspondence, Normal for your text, and Headings 1–3). Figure 1 uses the style Caption and Fig. 1 is placed at the end of the manuscript. The same is applied to tables (Aman et al., 2014; Aman and Bman, 2015) adipiscing elit. Mauris dictum, nibh ut condimentum pharetra, quam ligula varius est, sed vehicula massa erat ut metus. In eget metus lorem. Fusce vitae ante dictum, elementum sem non, lacinia dui. Integer tellus tortor, convallis et aliquam non, dictum vel mauris. Quisque maximus mollis dui, a mollis mauris vehicula in. Duis dui ligula, suscipit ac lectus vitae, fringilla euismod diam.

1 Introduction

As a key component of the atmospheric system, convective cloud processes and their representations over tropical regions introduce large uncertainty in numerical weather and climate model predictions (Betts and Jakob, 2002; Dai, 2006). To global climate model (GCMs) scales, we can point some unresolved or incorrect issues observed on modelled data over the tropics: a) the incorrect phasing of the precipitation diurnal cycle over land that favours models triggering precipitation too early in the day (Gentine et al., 2013); b) the position and often doubling of the Intertropical Convergence Zone (Hwang and Frierson, 2013); and c) the underestimation of rainfall over the Amazon forest (Huntingford et al., 2004). The tropical diurnal precipitation cycle representation has been studied for decades, using numerical models (Bechtold et al., 2004; Sato et al., 2009; Stratton and Stirling, 2012) and observational techniques (Itterly et al., 2016; Machado et al., 2002; Oliveira et al., 2016).

Given its unique tropical location, propensity for deep convection, and potential influence on the global circulation, several scientific campaigns have focused on convective cloud, aerosol transportation, and land-atmosphere interactions studies over the Amazon forest during the last 20 years (Machado et al., 2014; Martin et al., 2016; Silva Dias et al., 2002; Wendisch et al., 2016). Specific to Amazon basin convective studies, model treatments for shallow convection and the transition to deep convection have been identified as possible challenges to the correct representation of the diurnal cycle in GCMs (Khairoutdinov and Randall, 2006). Since convection is parameterized in GCMs and convection may range from smaller to

larger than the typical GCM grid resolution, the differences in the convective scale driven by large-scale circulation should then be taken into account in convection parametrization schemes and satellite-based rainfall retrievals (Rickenbach et al., 2002). This suggests that the differences between the organized, or larger areal coverage convective regimes and localized isolated convection, needs to be better understood for correct representation of convective processes from cloud-resolving models (CRM) to GCM parametrization scalings.

Improving and validating GCM convective parameterizations is challenging owing to an absence of direct, process-scale observations (e.g., updraft dynamics, particle size distributions) inside deep convective clouds that operate over a similar range of scales. Traditionally, convective dynamics have been informed by instrumented aircraft (Byers and Braham, 1949; LeMone and Zipser, 1980; Rosenfeld et al., 2006), but strong vertical air motions and practical flight operations considerations limits direct aircraft measurements in the more intense convective clouds. Recently, remote-sensing alternatives such as scanning, and zenith-pointing radar retrievals have been advanced to offset these observational deficiencies (Giangrande et al., 2013). Profiling radars have been shown to be an alternative for extended deployments and statistical deeper convective studies, providing reliable and high (temporal, vertical) resolution for vertical air motion retrievals (Heymsfield et al., 2010).

Recently, the GoAmazon2014/5 campaign (Martin et al., 2016) concluded a two-year deployment over Manaus and its surroundings, including an advanced complement of cloud and precipitation profiling instruments. This unique deployment offers several opportunities to investigate cloud lifecycle and environmental conditions sampled before and concurrent to cloud development, as well as the associated precipitation properties.

This study explores the controls on the diurnal rainfall in the Amazon basin. To accomplish this, we introduce unique atmospheric characteristics available during GoAmazon2014/5 observed before the diurnal cycle of convective precipitation (nocturnal periods before precipitating and non-precipitating days) to monitor potential differences in those controls, subsequent diurnal precipitation properties, and changes between seasonal regimes (dry and wet season). This is accomplished from a scale analysis standpoint, comparing the influence of the local cloud coverage and PBL characteristics versus the influence of the mesoscale convection pattern. The identification of such features and their contrasts between seasons allows us to better predict rainfall occurrence and develop better convective parameterizations for GCMs.

2 Data

The GoAmazon field campaign was conducted in 2014 and 2015. The main site (codename T3) was located in Manacapuru, state of Amazonas (latitude: -3.213, longitude: -60.598), roughly 80 km west of Manaus. Several instruments were deployed to T3 as part of the U.S. Department of Energy Atmospheric Radiation Measurement Program (ARM) Climate Research Facility (Ackerman and Stokes, 2003) Mobile Facility 1 (AMF1). Additional details on the ARM-T3 deployment and dataset collection is provided in (Giangrande et al., 2017).

A primary ARM data source used in this study is the Active Remote Sensing of Clouds (ARSCLs) Value-Added Product (VAP). This data product combines measurements from a ceilometer, a micro pulse lidar, and a vertically pointing W-Band (94 GHz) radar (Clothiaux et al., 2000). We use the cloud mask available in the ARSCL to derive cloud mean occurrences. The values were calculated averaging occurrences observed by height over our periods of observation and transitions modes.

5 Also, from ARM is the ECOR – eddy correlation flux measurement system, used to derive the turbulent kinetic energy; the SEBS – Surface Energy Balance System, used to compute the soil temperature means; the radiosondes launched 4 times a day (0, 6, 12, and 18 GMT) used to compute CAPE and CIN; and a ceilometer used to derive the Planetary Boundary Layer (PBL) height.

Rainfall observation is provided by an automatic weather station and using a radar to check for rainfall in the vicinities. The

10 SIPAM S-Band (2.2 GHz) radar is a single polarization, doppler weather radar performing a volume scan each 12 minutes, with a 2° beam width and radial resolution of 500 m. The SIPAM radar is located in Manaus and has a 240 km radius range.

For additional analysis, the GOES 10.4 μm brightness temperature data acquired over a 10° x 10° box centred on T3 was used to verify the occurrence of cold cloud tops that would indicate the presence of precipitating clouds around the studied region. GOES data is received and processed operationally by CPTEC/INPE since 1997 (Costa et al., 2018).

15 **3 Methodology**

The purpose for this study is to identify which controls from the previous day (e.g., nocturnal periods from the days preceding precipitation) are the better predictors for diurnal precipitation on the following days. To accomplish this, we first define a previous day 'nocturnal period' as the period between 0000 GMT and 1200 GMT (2000 LT to 0800 LT), and the subsequent 'diurnal period' as the period between 1200 GMT and 0000 GMT (0800 LT to 2000 LT) on the adjacent day.

20 From those definitions, we then categorized Amazon observations into two classes: a) days having no rain during the nocturnal period and no rain during the subsequent diurnal period; and b) days having no rain during the nocturnal period, but having rain observed during the subsequent diurnal period. We refer to these transitions as NR-NR (no rain to no rain) and NR-RR (no rain to rain), compromising a 24-hour period. Note that days having rain within the nocturnal period are removed from this analysis. Our intention is to identify possible controls during nocturnal periods that may trigger

25 precipitation in the next diurnal period. A visual depiction of this methodology is described in Figure 1.

We used a local weather station and a 1 km-horizontally gridded, 3 km-level CAPPI derived from the SIPAM S-Band radar to define precipitation events. A 50 x 50 km area centred at the GoAmazon2014/5 main facility (an area similar to a GCM grid space) was delineated (include a figure about the region?), and the reflectivity values greater than 25 dBZ were counted.

If more than 10% of the area presents reflectivity levels above the 25 dBZ threshold, we mark that event as rain. Moreover,

30 if the weather station reported a rainfall accumulation greater than 1mm during an hour, that event is also marked as rain. As we want to verify the nightly controls over the diurnal precipitation, events with rain during the 20LT to 08LT time window were discarded from our dataset.

Given that we want to verify the differences between regimes, we defined the wet season as the period between January and April and the dry season between June and September (needs to include references about the wet and dry season start). We used both years of data (2014 and 2015) in our analysis.

We extend our examination to the characteristics of the PBL and atmospheric profiles during the day using in-situ data. The mesoscale characteristics and cloud coverage were examined using infrared GOES data observed over a $10^\circ \times 10^\circ$ box centred at T3, from 20 LT to 08 LT.

4 Results

We start our investigation of the atmospheric conditions with the cloud observations acquired during the non-raining nocturnal period, using two different conditions: no-rain or rain observed during the subsequent diurnal period (from 08 to 20 LT), as explained in Figure 1. We compiled 51 NR-NR cases and 113 NR-RR cases during the wet season, and 148 NR-NR cases and 64 NR-RR cases during the dry season. For a better exhibition of the convection onset during the morning we extended the displayed period up to 12 LT. Cloud development is strongly attached to moisture availability and vertical motion. We propose that during the wet season, when high levels of moisture are observed the cloud development is a direct effect of the vertical movement. The dry season controls and hypothesis will be discussed later. We present the results in Figure 2, breaking our results by season (wet on the left panel and dry on the right) and transition. We focus our analysis in the lower part of the atmosphere (below the freezing level, which is found around 4.5 km as stated by the radiosonde data). This is due to limitation of the instrumentation, which provides better retrievals in the liquid phase, and because we expect only shallow clouds during non-raining nights (residual cirrus from the previous day cumulus clouds could also be expected, but we are not focusing on them in this analysis). We also present the absolute cloud occurrence difference between the modes on the bottom panel. Null (zero percent) cloud differences are marked in white.

Starting with the wet season results, we show that cloud occurrences above 15% are always observed from 22 LT to 06 LT during the NR-NR transition (top left panel) at some height level. From 2 to 3 km values often exceed 25%, and there is significant cloud coverage near the surface from 00 LT to 04 LT. As the sun rises (around 06 LT) until 07 LT some low-level cloud activity is observed, surpassing 25% at some points. There is some intense, but shallow convection observed after 10 LT, with cloud occurrences over 40%. During the raining mode (middle left panel) the overall cloud coverage is lower, and until 06 LT cloud occurrences rarely exceeds 10% up to 2 km. From 02 LT to 06 LT the cloud coverage between 2 and 4 km presents the higher values observed until the start of convection, which is observed around 10 LT. The convective activity presented at the sunrise is weaker than the NR-NR mode, but after 10 LT cloud occurrence exceeds 45% and its 30% contour height reaches 3 km. Note that since we extend our period of study from 08 LT to 12 LT there will be raining clouds contaminating these results after 08 LT, for all transition modes and seasons. The absolute difference (bottom left panel) shows that from 22 LT to 04 LT the non-raining mode presents higher cloud occurrence throughout the whole

column, with differences around 20%, which happens also frequently between 06 LT and 10 LT from the surface and 1.5 km and from 3 to 4 km. After 10 LT the NR-RR mode shows the maximum negative cloud differences, reaching -25%.

We suggest that this higher cloud occurrence during the night would consume energy that might have been available for convection during the next day, and cloud coverage during early mornings (with values over 30% observed between 05 and 08 LT near the surface) would prevent surface heating by blocking the incoming solar radiation. On the other hand, the increase in the incidence of solar radiation during NR-RR modes generates surface heat that would favour convective development, thus leading to precipitation. This behaviour was discussed from an energy budget standpoint in (Machado, 2000), where is shown that the surface loses more energy than receives in convective events, therefore there is less energy available at surface after a cloudy period. This also may be an indication that precipitating convection during the wet season are more prone to be triggered by local effects (such as surface heating) than large-scale flow. This physical cloud control mechanism shows the main feature, during the wet season, that control rainfall in Amazonas. The improvement of shallow convective parameterization is the key feature to have a better rainfall representation in continental tropical region.

The dry season (left panels) results show that this season presents almost no cloud activity during the nights – their contrast with the higher cloud coverage observed during the wet season are clear. When breaking down the results by transitions, the NR-NR mode hardly shows cloud occurrence values between over 5%. Only during the sunrise and after 10 LT that those values reaches values over 15%. The NR-RR transition shows a more significant cloud coverage above 1 km and some surface clouds after 08 LT, which during the NR-NR mode have occurrences below 5%. The calculated differences show that the raining mode is predominantly cloudier than the NR-RR mode (most differences observed are negative), but these differences are subtle in comparison with those observed during the wet season. After the onset of convection and precipitation, around 10 LT, the behaviour of the observed wet and dry season differences is similar. As oppose to the wet season, the dry season NR-RR mode is cloudier during most of the nocturnal period on all levels observed.

The cloud coverage has a direct impact over the soil temperature. During a cloudy night there is a net increase of the longwave radiation at the surface, since clouds absorbs the upwelling radiation and reemits it (greenhouse effect). Figure 3 presents the evolution of the mean soil temperature during the night. The panel starts at 20 LT, when the temperature is 1 °C lower on average during the wet season (solid lines) than on the dry season (dashed lines). The wet season NR-NR (black lines) mode presents a slighter mean temperature in the beginning of the night, as expected from the radiative process involved during a cloudier situation. The wet season NR-NR and NR-RR temperatures equalize around 04 LT, and from 06 LT, roughly the sunrise time, the raining mode soil temperature becomes a little warmer, since the lower cloud coverage during the sunrise on the NR-RR mode allows more shortwave radiation to reach the soil. The dry season soil temperatures present the same pattern between the NR-RR and NR-RR modes, with the NR-RR one being slightly warmer.

In Figure 4 we present the thermodynamic parameters CAPE (convective available potential energy) and CIN (convective inhibition) using data derived from the nocturnal (20, 02, and 08 LT) radiosondes launched at T3. The boxplots were constructed to display the minimum, lower quartile, median, upper quartile, and maximum values. The wet season CAPE results (upper-left panel) display a reduction of the potential energy from 20 to 02 LT during the NR-NR transition (grey

boxes), while the NR-RR mode results (blue boxes) are practically the same for these two measurements. This CAPE reducing between the two first observations can be explained by the energy consumption by convection, since the cloudier period is found between 22 and 02 LT during the NR-NR transition. The NR-NR 20 LT CAPE is the highest one, leading to an increase of the cloud coverage, which consumes the energy, thus decreasing the CAPE in the next sounding. Between 02 and 08 LT there is an increase of the CAPE for both NR-NR and NR-RR modes during the wet season, probably due to the surface heating and the increase of the surface temperature after the sunrise. CAPE values are higher for the NR-RR mode during the 02 and 08 LT soundings. During the 20 LT one, the non-raining mode have a higher upper quartile value and maximum value, albeit the medians are quasi-identical between the modes. The dry season (upper-right panel) plots show higher CAPE values during the 08 LT sounding than the wet season, when comparing mode by mode. These results are compatible with the higher soil temperature observed during the dry season. The energy decrease in the NR-NR mode between 20 and 02 LT is less pronounced than the one observed in the wet season. The NR-RR changes observed between 20 and 02 LT are subtle: a slightly increase of the upper quartile value and the decreasing of the maximum value. An explanation for the similarities between the 20 and 02 LT results, for both modes, and their differences in comparison with the wet season results, is the lower cloud coverage observed during the dry season. The 02 LT sounding values are similar for the dry and wet seasons, for both NR-NR and NR-RR transitions. The wet season CIN (bottom-left panel) shows that the convective inhibition is less intense than those observed during the dry season (bottom-right panel), for all times and transitions. For both seasons the largest inhibitions are displayed during the 02 LT sounding, for the NR-NR mode.

As we move forward in time in our analysis, we will discuss the characteristics of the planetary boundary layer (PBL), starting with the Ceilometer-derived PBL height, as shown in Figure 5. As expected, the wet season, being the season with most convective activity overall, presents lower PBL heights, since cloud development implies a lower PBL. During the wet season, the distinction between the NR-NR and NR-RR transitions begins to appear at 08 LT. The maximum PBL height (approximately 1000 m) is reached around the local noon for the NR-RR transition, whereas the NR-NR maximum is 500 m higher and reached 2 hours later. Both height and time differences observed can be explained by the larger convective development that occurs preceding rainfall in the wet season. With moisture freely available during the wet season, any condition that favours cloud development such as surface heating or local instabilities can trigger convection, thus lowering the PBL. Moreover, the rainfall occurrence distribution (Figure 6) shows that the precipitation occurrences are more well-spread during the day than the dry season distribution, which presents a distinct peak around noon. The dry season observed PBL heights are higher than the wet season ones, and even the NR-RR mode of the dry season presents a higher PBL than the wet season NR-NR mode. Not only the low number of NR-RR events (64 during the dry season versus 113 during the wet season) explains this difference, but the diurnal cycle of the rainfall occurrence during the dry season helps determine this behaviour.

The ECOR derived Turbulent Kinetic Energy (TKE) results (Figure 7) show that the dry season presents higher values of TKE than the wet season. Clear differences between the wet season modes are observed, with the NR-RR mode having the higher values of TKE, reaching $1.2 \text{ m}^2\text{s}^{-2}$ around the local noon. The NR-NR and NR-RR wet season curves show

significant different values since 06 LT, showing that turbulence is a key factor in triggering deeper clouds and precipitation. On the other hand, the dry season TKE is similar for both NR-NR and NR-RR modes, indicating that local turbulence does not play an important role on the precipitating cloud development during the dry season.

With the results presented so far, we cannot explain the dry season precipitation onset based on local factors. The dry season precipitation characteristics observed during the two years of the GoAmazon experiment (Ghate and Kollias, 2016) indicate a relationship between large-scale moisture advection and precipitation, as well as local land-atmosphere interactions triggering the transition from shallow to deep convection. During the wet season surface heating is easily transformed in surface latent heating, however, the dry season, being much drier, the solar energy is mainly transformed in sensible heating (Fu and Li, 2004).

To further investigate the influences of local effects versus the influence of the mesoscale pattern, we calculated the mean field of the GOES 10.4 μm brightness temperatures observed over a $10^\circ \times 10^\circ$ box centred at T3 during the nocturnal period. Furthermore, we calculated the CDF and the PDF of these brightness temperatures, grouped in 3h intervals and separated by transition type and season.

Figure 8 presents the mean brightness temperature field during the nocturnal period (2000 LT – 0800 LT) observed over a $10^\circ \times 10^\circ$ box centred at T3 (the cross mark in each panel). The differences of the convective activity between NR-NR and NR-RR transitions during wet and dry seasons are well represented: convection is more intense during the wet season (top panels), and it is observed around the whole domain. No significative difference is noted between NR-NR and NR-RR days during the wet season around T3: temperatures below 275 K can be observed in more than 90% of the region for both transition types. During the dry season the NR-RR transition (bottom left panel) presents warmer temperatures, and values above 280 K comprehend almost the totality of the region. The NR-RR transition (bottom right panel) presents colder temperatures, 5 to 10 K lower than the NR-NR transition overall. This result shows that the NR-RR and NR-NR days are mainly characterized by meso-large scale features than local convective processes.

The mean behaviour observed in Figure 8 can be detailed breaking the observations in fixed time intervals. We present on Figure 9 the probability distribution and the cumulative distribution function of the GOES-13 10.4 μm brightness temperatures grouped into 3 h time steps, for the nocturnal period. This analysis helps us to understand the evolution of the convective systems around our region of study and identify the differences presented between seasons and transitions more clearly. All distributions presented in Figure 9 are left-skewed unimodal distributions, with peaks between 285 K and 295 K. Wet season distributions (black lines) are similar for both transition types, for all time intervals analysed. Values observed for the wet season are generally lower (colder temperatures) than those observed in the dry season, indicating a stronger convective activity throughout the domain independent of transition type or time interval. Dry season distributions are quite different during NR-NR and NR-RR events, with a larger incidence of higher values (warmer temperatures) during NR-RR transitions.

The wet season mean cloud field similarities are even better represented in the CDFs (Figure 10), indicating that the mean cloud field is similar during the night regardless of precipitation observed during the subsequent day. In other words, the

mesoscale mean convective characteristics are the same for both transition modes, and the development of precipitating clouds observed at T3 during the wet season appears to be influenced mostly by local factors, as discussed before. In contrast, the dry season distributions are quite different: the 25th percentiles of the NR-RR transitions if often reached around 250 K, while for the NR-NR transitions the Q1 value lies around 280 K. The NR-NR CDFs are very similar for all time intervals, but the differences between them and the NR-RR CDFs increase with time. This indicates that the mean cloud field is intensified as time passes, and the convection becomes deeper during the night, leading to precipitating clouds in the next day. The dry season NR-RR curves also show even colder values than both the wet season curves from 23 LT on, which means that when precipitating convection happens during the dry season it tends to be stronger than the wet season, as already observed in several studies (Itterly et al., 2016; Tanaka et al., 2014). The difference between the seasons and the results presented before (with local observations) show that the dry season precipitation is controlled directly by mesoscale circulation and local effects are neglectable.

5 Conclusions

In this paper we present a new approach on how convection and its transition to precipitation is developed over Central Amazon. We break down our results based on season – wet and dry – and 2 modes of transition: non-raining nights to non-raining days and non-raining nights to raining days. It is shown that during the wet season the local influences are the key effect in the occurrence of rainfall over our region of study. During the dry season mesoscale factors are more important and dominate the development of the precipitation observed.

The results presented here show that during the wet season the diurnal precipitation is modulated mainly by the cloud coverage during the night. Since cloud development is associated with vertical motion and moisture availability, and since during the wet season moisture is freely available, we conclude that the nocturnal vertical motion is responsible for the cloud development. Therefore, the wet season NR-RR transition has a higher subsidence during the night (from 22 to 04 LT) and right after the sunrise (from 06 to 10 LT), suppressing cloud formation during the first hours of the morning, which allows the surface to receive more solar energy. This is corroborated by the soil temperature observations. Since there is enough moisture available, the heating is transformed in latent heating building convective cells that will precipitate later during the day. However, in the wet season, nights with dominant upward motion will inhibit convection during the day, because the clouds formed during the night will reduce solar radiation at the surface during the first hours of the day. If during the wet season a clear distinction during the night is observed between the NR-NR and NR-RR days, for the dry season no significant signal is observed. That indicates that the local processes are not the key feature controlling the transition from shallow convection to rainfall when moisture is scarcer. The convective activity also is on average more intense during the wet season than the dry season for both types of transitions.

The analysis of the PBL attributes shows that turbulence does not play a major role on the dry season – there is no distinguishable features between the NR-NR and the NR-RR transitions. On the other hand, the distinction between the

transitions are clear during the wet season – both the turbulent kinetic energy and PBL heights have different values between raining and non-raining modes.

The satellite data analysis shows that during the dry season precipitation is observed at T3 during days where cloud activity is seen throughout all its surroundings during the nights, indicating a mesoscale modulation in the convection for this season.

5 There is a clear difference in the PDFs and CDFs between the raining modes. On the other hand, wet season brightness temperatures distributions are similar for NR-NR and NR-RR transitions.

These results show that models and parameterizations must consider different formulations based on the seasonal cycle to correctly resolve the precipitating convection over central Amazon. A convective parameterization scheme using only local or small-scale interactions will give poor results during the dry season. On the other hand, larger mass-flux convergence

10 approaches will not perform well during the wet season, triggering precipitation at wrong times or quantifying it erroneously.

References

- Ackerman, T. P. and Stokes, G. M.: The Atmospheric Radiation Measurement Program, *Phys. Today*, 56(1), 38–44, doi:10.1063/1.1554135, 2003.
- 15 Bechtold, P., Chaboureau, J.-P., Beljaars, A. C. M., Betts, A. K., Köhler, M., Miller, M. and Redelsperger, J.-L.: The simulation of the diurnal cycle of convective precipitation over land in a global model, *Q. J. R. Meteorol. Soc.*, 130(604), 3119–3137, doi:10.1256/qj.03.103, 2004.
- Betts, A. K. and Jakob, C.: Evaluation of the diurnal cycle of precipitation, surface thermodynamics, and surface fluxes in the ECMWF model using LBA data, *J. Geophys. Res.*, 107(D20), 8045, doi:10.1029/2001JD000427, 2002.
- 20 Byers, H. R. and Braham, R. R.: *The Thunderstorms*, U.S. Govt. Printing Office, Washington., 1949.
- Clothiaux, E. E., Ackerman, T. P., Mace, G. G., Moran, K. P., Marchand, R. T., Miller, M. A. and Martner, B. E.: Objective Determination of Cloud Heights and Radar Reflectivities Using a Combination of Active Remote Sensors at the ARM CART Sites, *J. Appl. Meteorol.*, 39(5), 645–665, doi:10.1175/1520-0450(2000)039<0645:ODOCHA>2.0.CO;2, 2000.
- Costa, S. M. S., Negri, R. G., Ferreira, N. J., Schmit, T. J., Arai, N., Flauber, W., Ceballos, J., Vila, D., Rodrigues, J.,
- 25 Machado, L. A., Pereira, S., Bottino, M. J., Sismanoglu, R. A. and Langden, P.: A Successful Practical Experience with Dedicated Geostationary Operational Environmental Satellites GOES-10 and -12 Supporting Brazil, *Bull. Am. Meteorol. Soc.*, 99(1), 33–47, doi:10.1175/BAMS-D-16-0029.1, 2018.
- Dai, A.: Precipitation characteristics in eighteen coupled climate models, *J. Clim.*, 19(18), 4605–4630, doi:10.1175/JCLI3884.1, 2006.
- 30 Fu, R. and Li, W.: The influence of the land surface on the transition from dry to wet season in Amazonia, *Theor. Appl. Climatol.*, 78(1–3), 97–110, doi:10.1007/s00704-004-0046-7, 2004.
- Gentine, P., Betts, A. K., Lintner, B. R., Findell, K. L., van Heerwaarden, C. C. and D’Andrea, F.: A Probabilistic Bulk

- Model of Coupled Mixed Layer and Convection. Part II: Shallow Convection Case, *J. Atmos. Sci.*, 70(6), 1557–1576, doi:10.1175/JAS-D-12-0146.1, 2013.
- Ghate, V. P. and Kollias, P.: On the Controls of Daytime Precipitation in the Amazonian Dry Season, *J. Hydrometeorol.*, 17(12), 3079–3097, doi:10.1175/JHM-D-16-0101.1, 2016.
- 5 Giangrande, S. E., Collis, S., Straka, J., Protat, A., Williams, C., Krueger, S., Giangrande, S. E., Collis, S., Straka, J., Protat, A., Williams, C. and Krueger, S.: A Summary of Convective-Core Vertical Velocity Properties Using ARM UHF Wind Profilers in Oklahoma, *J. Appl. Meteorol. Climatol.*, 52(10), 2278–2295, doi:10.1175/JAMC-D-12-0185.1, 2013.
- Giangrande, S. E., Feng, Z., Jensen, M. P., Comstock, J. M., Johnson, K. L., Toto, T., Wang, M., Burleyson, C., Bharadwaj, N., Mei, F., Machado, L. A. T., Manzi, A. O., Xie, S., Tang, S., Silva Dias, M. A. F., de Souza, R. A. F., Schumacher, C. and
- 10 Martin, S. T.: Cloud characteristics, thermodynamic controls and radiative impacts during the Observations and Modeling of the Green Ocean Amazon (GoAmazon2014/5) experiment, *Atmos. Chem. Phys.*, 17(23), 14519–14541, doi:10.5194/acp-17-14519-2017, 2017.
- Heymsfield, G. M., Tian, L., Heymsfield, A. J., Li, L. and Guimond, S.: Characteristics of Deep Tropical and Subtropical Convection from Nadir-Viewing High-Altitude Airborne Doppler Radar, *J. Atmos. Sci.*, 67, 285–308, doi:10.1175/2009JAS3132.1, 2010.
- 15 Huntingford, C., Harris, P. P., Gedney, N., Cox, P. M., Betts, R. A., Marengo, J. A. and Gash, J. H. C.: Using a GCM analogue model to investigate the potential for Amazonian forest dieback, *Theor. Appl. Climatol.*, 78(1–3), 177–185, doi:10.1007/s00704-004-0051-x, 2004.
- Hwang, Y.-T. and Frierson, D. M. W.: Link between the double-Intertropical Convergence Zone problem and cloud biases
- 20 over the Southern Ocean, *Proc. Natl. Acad. Sci.*, 110(13), 4935–4940, doi:10.1073/pnas.1213302110, 2013.
- Itterly, K. F., Taylor, P. C., Dodson, J. B. and Tawfik, A. B.: On the sensitivity of the diurnal cycle in the Amazon to convective intensity, *J. Geophys. Res. Atmos.*, 121(14), 8186–8208, doi:10.1002/2016JD025039, 2016.
- Khairoutdinov, M. and Randall, D.: High-Resolution Simulation of Shallow-to-Deep Convection Transition over Land, *J. Atmos. Sci.*, 63(12), 3421–3436, doi:10.1175/JAS3810.1, 2006.
- 25 LeMone, M. A. and Zipser, E. J.: Cumulonimbus Vertical Velocity Events in GATE. Part I: Diameter, Intensity and Mass Flux, *J. Atmos. Sci.*, 37(11), 2444–2457, doi:10.1175/1520-0469(1980)037<2444:CVVEIG>2.0.CO;2, 1980.
- Machado, L. A. T.: The Amazon Energy Budget Using the ABLE-2B and FluAmazon Data, *J. Atmos. Sci.*, 57(18), 3131–3144, doi:10.1175/1520-0469(2000)057<3131:TAEBUT>2.0.CO;2, 2000.
- Machado, L. A. T., Laurent, H. and Lima, A. A.: Diurnal march of the convection observed during TRMM-WETAMC/LBA,
- 30 *J. Geophys. Res.*, 107(D20), 8064, doi:10.1029/2001JD000338, 2002.
- Machado, L. A. T., Silva Dias, M. A. F., Morales, C., Fisch, G., Vila, D., Albrecht, R., Goodman, S. J., Calheiros, A. J. P., Biscaro, T., Kummerow, C., Cohen, J., Fitzjarrald, D., Nascimento, E. L., Sakamoto, M. S., Cunningham, C., Chaboureau, J.-P., Petersen, W. A., Adams, D. K., Baldini, L., Angelis, C. F., Sapucci, L. F., Salio, P., Barbosa, H. M. J., Landulfo, E., Souza, R. A. F., Blakeslee, R. J., Bailey, J., Freitas, S., Lima, W. F. A., Tokay, A., Machado, L. A. T., Dias, M. A. F. S.,

- Morales, C., Fisch, G., Vila, D., Albrecht, R., Goodman, S. J., Calheiros, A. J. P., Biscaro, T., Kummerow, C., Cohen, J., Fitzjarrald, D., Nascimento, E. L., Sakamoto, M. S., Cunningham, C., Chaboureaud, J.-P., Petersen, W. A., Adams, D. K., Baldini, L., Angelis, C. F., Sapucci, L. F., Salio, P., Barbosa, H. M. J., Landulfo, E., Souza, R. A. F., Blakeslee, R. J., Bailey, J., Freitas, S., Lima, W. F. A. and Tokay, A.: The CHUVA Project: How Does Convection Vary across Brazil?, *Bull. Am. Meteorol. Soc.*, 95(9), 1365–1380, doi:10.1175/BAMS-D-13-00084.1, 2014.
- 5 Martin, S. T., Artaxo, P., Machado, L., Manzi, A. O., Souza, R. A. F., Schumacher, C., Wang, J., Biscaro, T., Brito, J., Calheiros, A., Jardine, K., Medeiros, A., Portela, B., de Sá, S. S., Adachi, K., Aiken, A. C., Albrecht, R., Alexander, L., Andreae, M. O., Barbosa, H. M. J., Buseck, P., Chand, D., Comstock, J. M., Day, D. A., Dubey, M., Fan, J., Fast, J., Fisch, G., Fortner, E., Giangrande, S., Gilles, M., Goldstein, A. H., Guenther, A., Hubbe, J., Jensen, M., Jimenez, J. L., Keutsch, F. N., Kim, S., Kuang, C., Laskin, A., McKinney, K., Mei, F., Miller, M., Nascimento, R., Pauliquevis, T., Pekour, M., Peres, J., Petäjä, T., Pöhlker, C., Pöschl, U., Rizzo, L., Schmid, B., Shilling, J. E., Silva Dias, M. A., Smith, J. N., Tomlinson, J. M., Tóta, J., Wendisch, M., Martin, S. T., Artaxo, P., Machado, L., Manzi, A. O., Souza, R. A. F., Schumacher, C., Wang, J., Biscaro, T., Brito, J., Calheiros, A., Jardine, K., Medeiros, A., Portela, B., Sá, S. S. de, Adachi, K., Aiken, A. C., Albrecht, R., Alexander, L., Andreae, M. O., Barbosa, H. M. J., Buseck, P., Chand, D., Comstock, J. M., Day, D. A., Dubey, M., Fan, J., Fast, J., Fisch, G., Fortner, E., Giangrande, S., Gilles, M., Goldstein, A. H., Guenther, A., Hubbe, J., Jensen, M., Jimenez, J. L., Keutsch, F. N., Kim, S., Kuang, C., Laskin, A., McKinney, K., et al.: The Green Ocean Amazon Experiment (GoAmazon2014/5) Observes Pollution Affecting Gases, Aerosols, Clouds, and Rainfall over the Rain Forest, *Bull. Am. Meteorol. Soc.*, BAMS-D-15-00221.1, doi:10.1175/BAMS-D-15-00221.1, 2016.
- 10 Oliveira, R., Maggioni, V., Vila, D. and Morales, C.: Characteristics and diurnal cycle of GPM rainfall estimates over the Central Amazon region, *Remote Sens.*, 8(7), doi:10.3390/rs8070544, 2016.
- Rickenbach, T. M., Ferreira, R. N., Halverson, J. B., Herdies, D. L. and Silva Dias, M. A. F.: Modulation of convection in the southwestern Amazon basin by extratropical stationary fronts, *J. Geophys. Res.*, 107(D20), 8040, doi:10.1029/2000JD000263, 2002.
- Rosenfeld, D., Woodley, W. L., Krauss, T. W. and Makitov, V.: Aircraft Microphysical Documentation from Cloud Base to Anvils of Hailstorm Feeder Clouds in Argentina, *J. Appl. Meteorol. Climatol.*, 45(9), 1261–1281, doi:10.1175/JAM2403.1, 2006.
- 25 Sato, T., Miura, H., Satoh, M., Takayabu, Y. N. and Wang, Y.: Diurnal cycle of precipitation in the tropics simulated in a global cloud-resolving model, *J. Clim.*, 22(18), 4809–4826, doi:10.1175/2009JCLI2890.1, 2009.
- Silva Dias, M. A. F., Rutledge, S., Kabat, P., Silva Dias, P. L., Nobre, C., Fisch, G., Dolman, A. J., Zipser, E., Garstang, M., Manzi, A. O., Fuentes, J. D., Rocha, H. R., Marengo, J., Plana-Fattori, A., Sá, L. D. A., Alvalá, R. . C. S., Andreae, M. O., Artaxo, P., Gielow, R. and Gatti, L.: Cloud and rain processes in a biosphere-atmosphere interaction context in the Amazon Region, *J. Geophys. Res.*, 107(D20), 8072, doi:10.1029/2001JD000335, 2002.
- 30 Stratton, R. A. and Stirling, A. J.: Improving the diurnal cycle of convection in GCMs, *Q. J. R. Meteorol. Soc.*, 138(666), 1121–1134, doi:10.1002/qj.991, 2012.

Tanaka, L. M. D. S., Satyamurty, P. and Machado, L. A. T.: Diurnal variation of precipitation in central Amazon Basin, *Int. J. Climatol.*, 34(13), 3574–3584, doi:10.1002/joc.3929, 2014.

Wendisch, M., Pöschl, U., Andreae, M. O., Machado, L. A. T., Albrecht, R., Schlager, H., Rosenfeld, D., Martin, S. T., Abdelmonem, A., Afchine, A., Araújo, A., Artaxo, P., Aufmhoff, H., Barbosa, H. M. J., Borrmann, S., Braga, R., Buchholz,
5 B., Cecchini, M. A., Costa, A., Curtius, J., Dollner, M., Dorf, M., Dreiling, V., Ebert, V., Ehrlich, A., Ewald, F., Fisch, G.,
Fix, A., Frank, F., Fütterer, D., Heckl, C., Heidelberg, F., Hüneke, T., Jäkel, E., Järvinen, E., Jurkat, T., Kanter, S., Kästner,
U., Kenntner, M., Kesselmeier, J., Klimach, T., Knecht, M., Kohl, R., Kölling, T., Krämer, M., Krüger, M., Krisna, T. C.,
Lavric, J. V., Longo, K., Mahnke, C., Manzi, A. O., Mayer, B., Mertes, S., Minikin, A., Molleker, S., Münch, S., Nillius, B.,
Pfeilsticker, K., Pöhlker, C., Roiger, A., Rose, D., Rosenow, D., Sauer, D., Schnaiter, M., Schneider, J., Schulz, C., de
10 Souza, R. A. F., Spanu, A., Stock, P., Vila, D., Voigt, C., Walser, A., Walter, D., Weigel, R., Weinzierl, B., Werner, F.,
Yamasoe, M. A., Ziereis, H., Zinner, T., Zöger, M., Wendisch, M., Pöschl, U., Andreae, M. O., Machado, L. A. T., Albrecht,
R., Schlager, H., Rosenfeld, D., Martin, S. T., Abdelmonem, A., Afchine, A., Araújo, A., Artaxo, P., Aufmhoff, H., Barbosa,
H. M. J., Borrmann, S., Braga, R., Buchholz, B., Cecchini, M. A., Costa, A., et al.: The ACRIDICON-CHUVA campaign:
Studying tropical deep convective clouds and precipitation over Amazonia using the new German research aircraft HALO,
15 *Bull. Am. Meteorol. Soc.*, BAMS-D-14-00255.1, doi:10.1175/BAMS-D-14-00255.1, 2016.

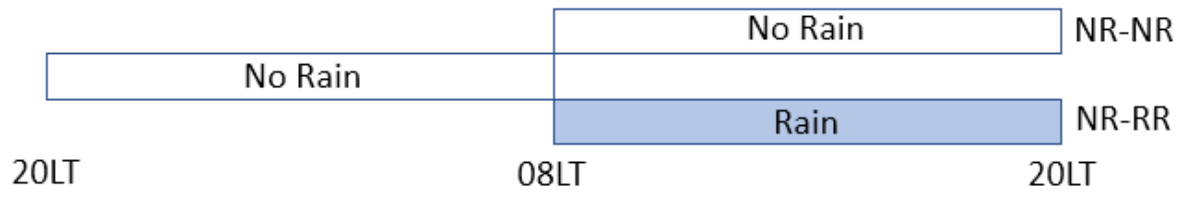


Figure 1: Visual depiction of the transition modes studied.

5

Cloud occurrence and absolute cloud occurrence difference

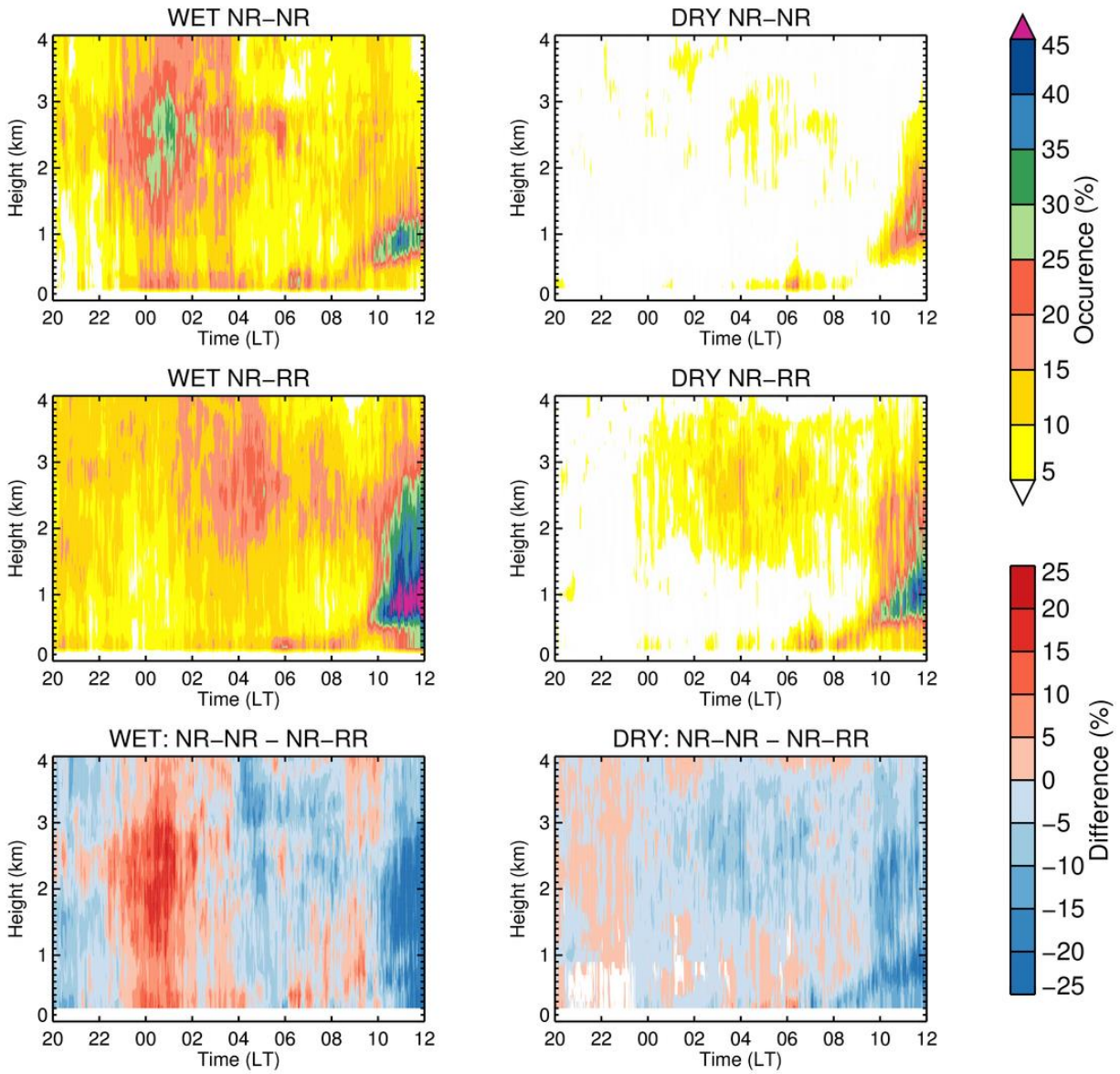


Figure 2: Cloud occurrence and absolute differences between non-raining and raining transitions, for wet and dry seasons.

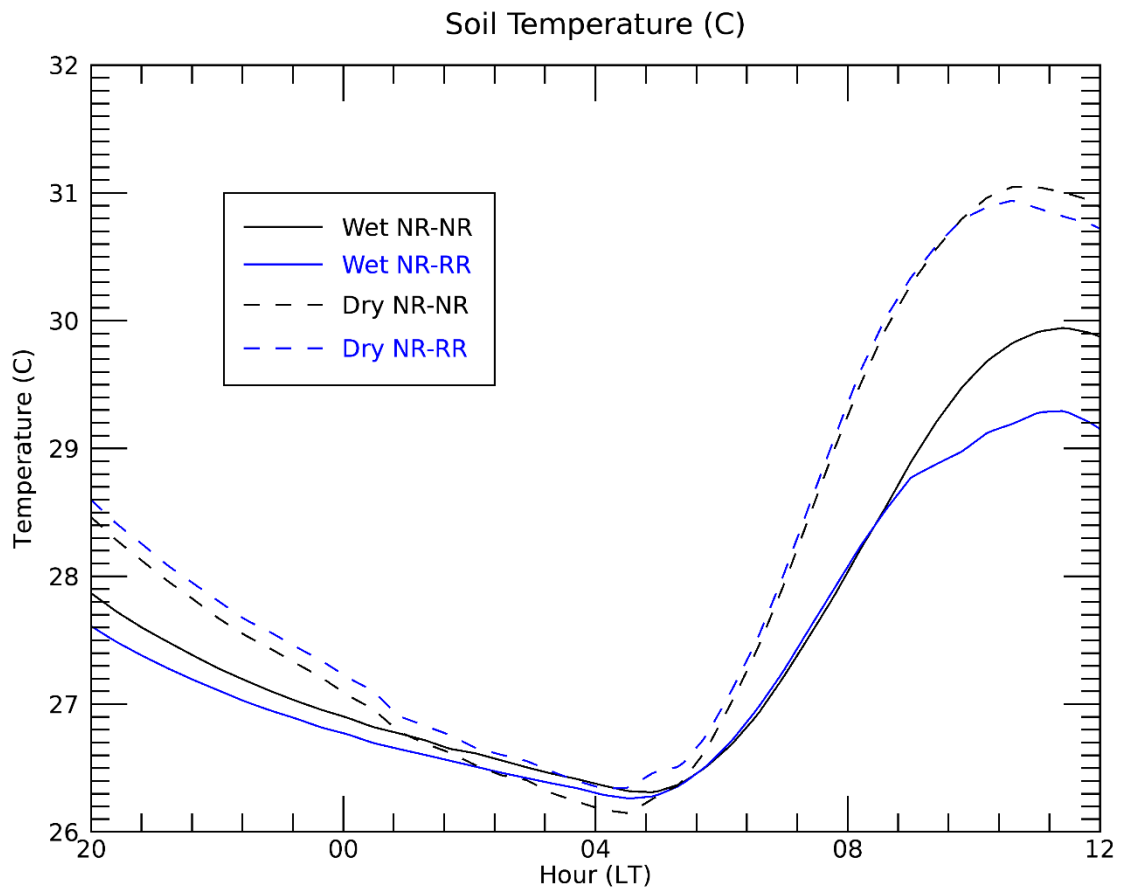


Figure 3: Soil temperature as measured by SEBS

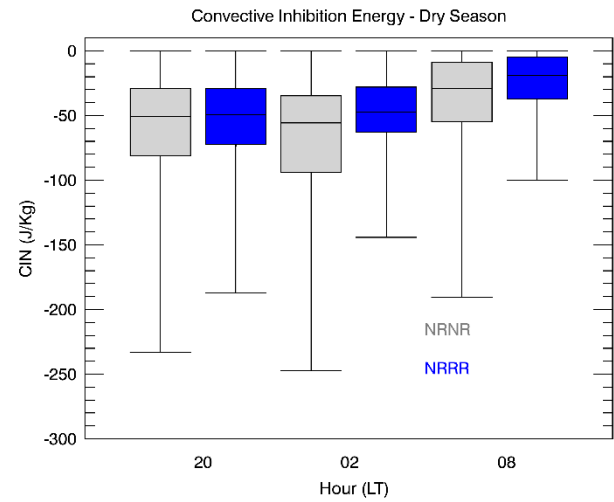
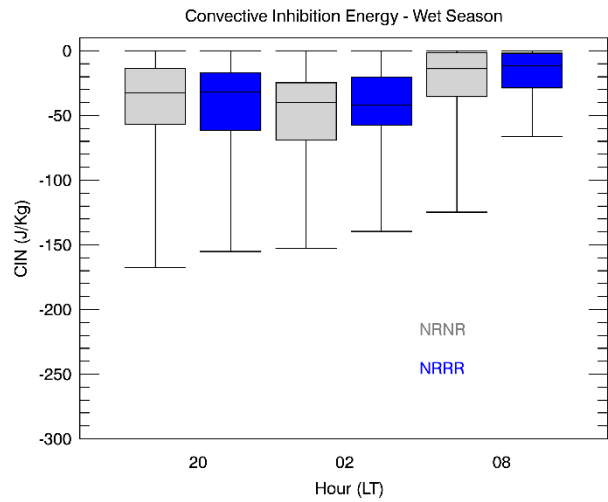
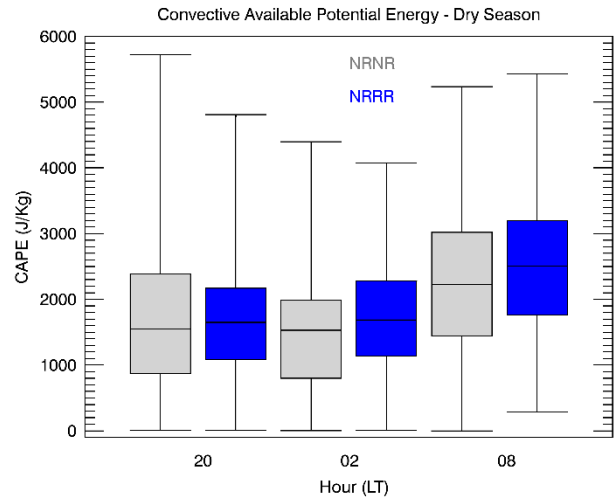
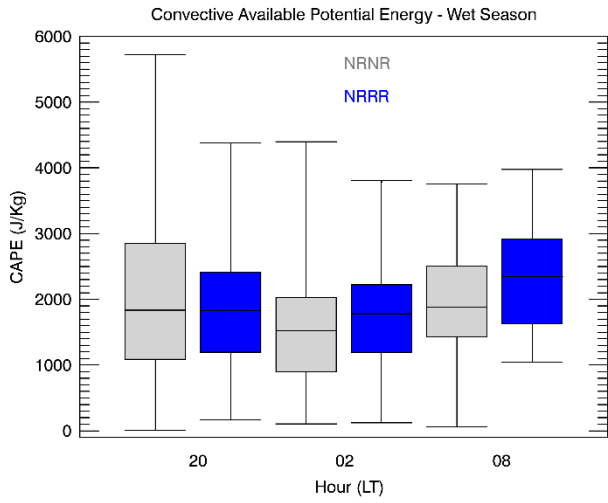


Figure 4: CAPE and CIN derived with the radiosondes during the nocturnal period at T3

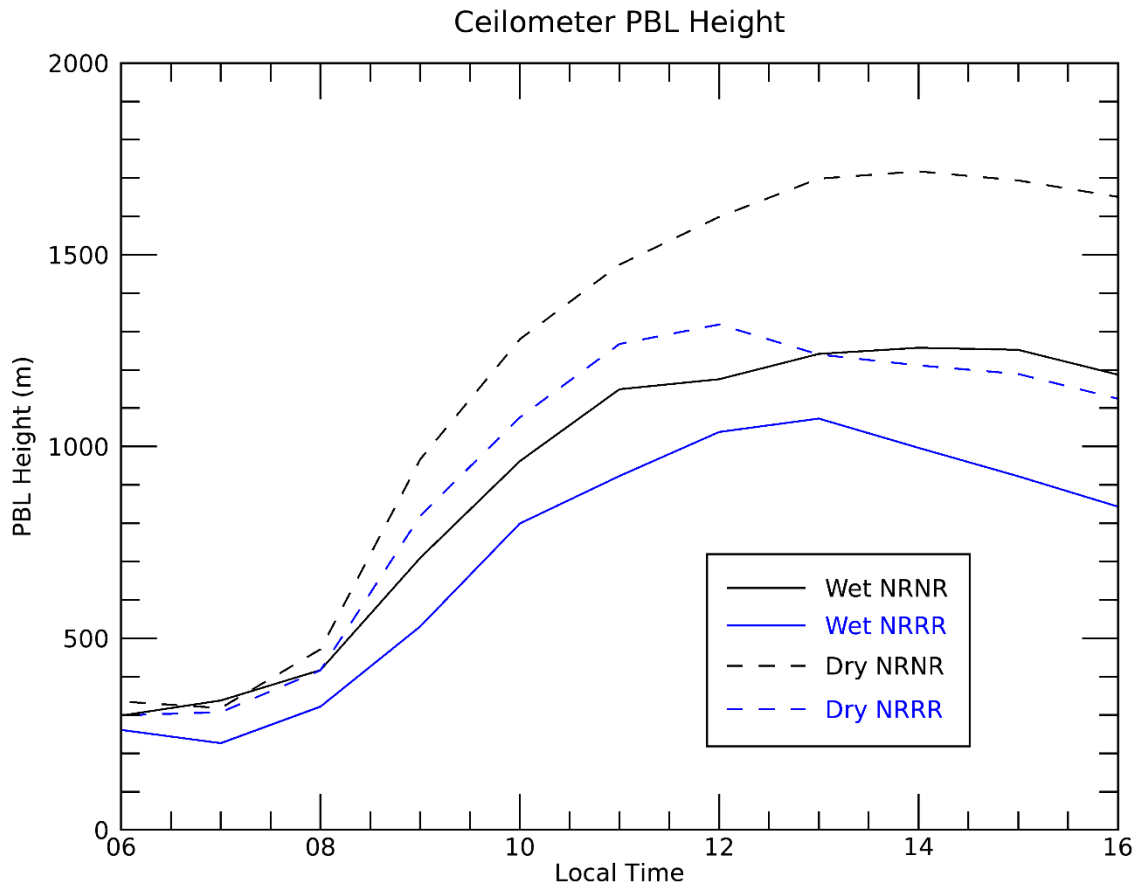


Figure 5: Planetary Boundary Layer height derived with the ceilometer

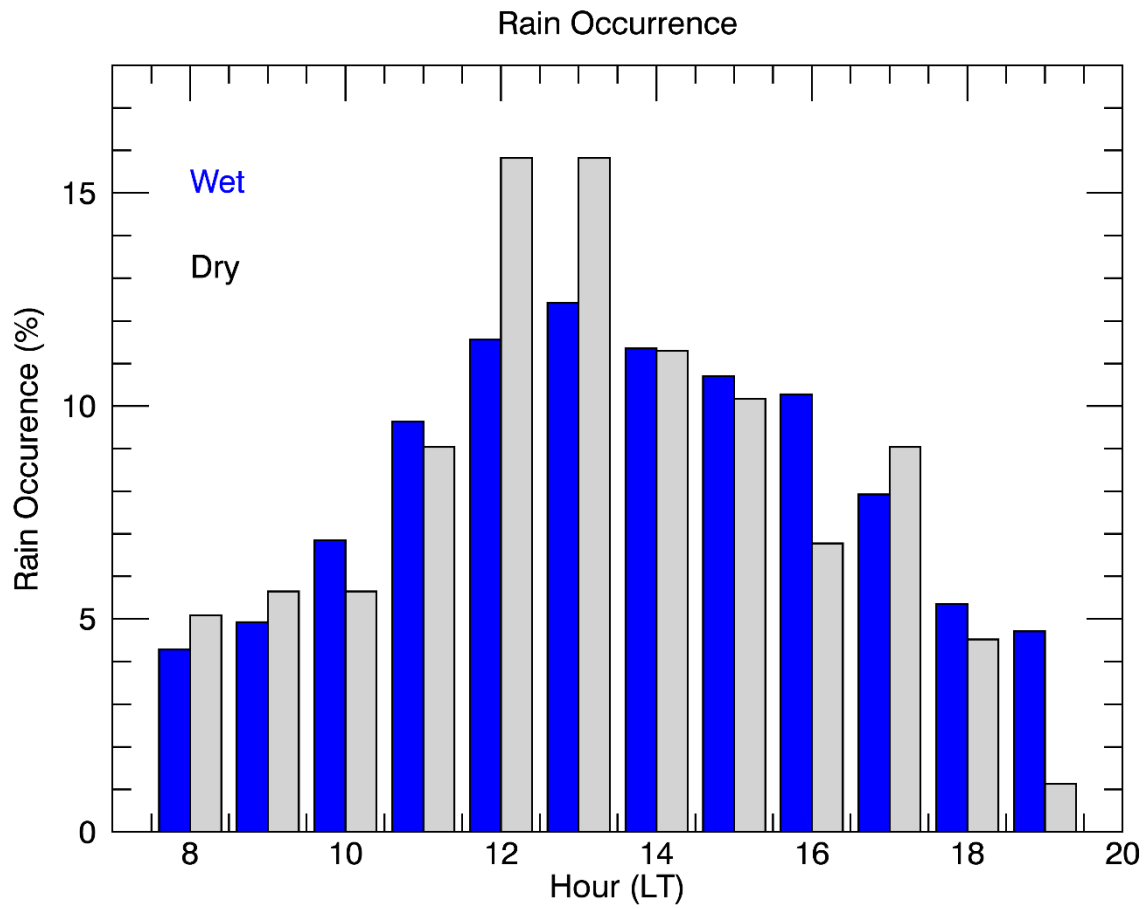


Figure 6: Rainfall occurrence distribution per hour

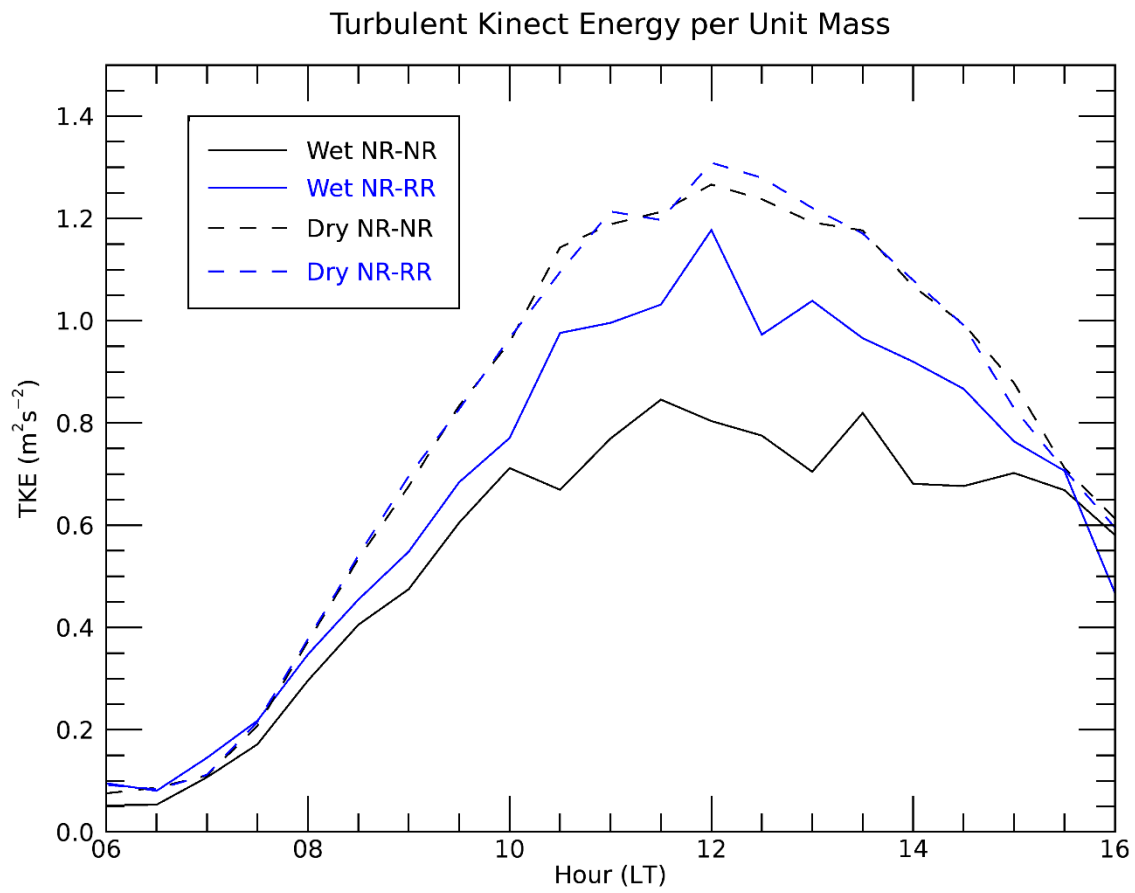


Figure 7: Turbulent kinetic energy derived with the ECOR

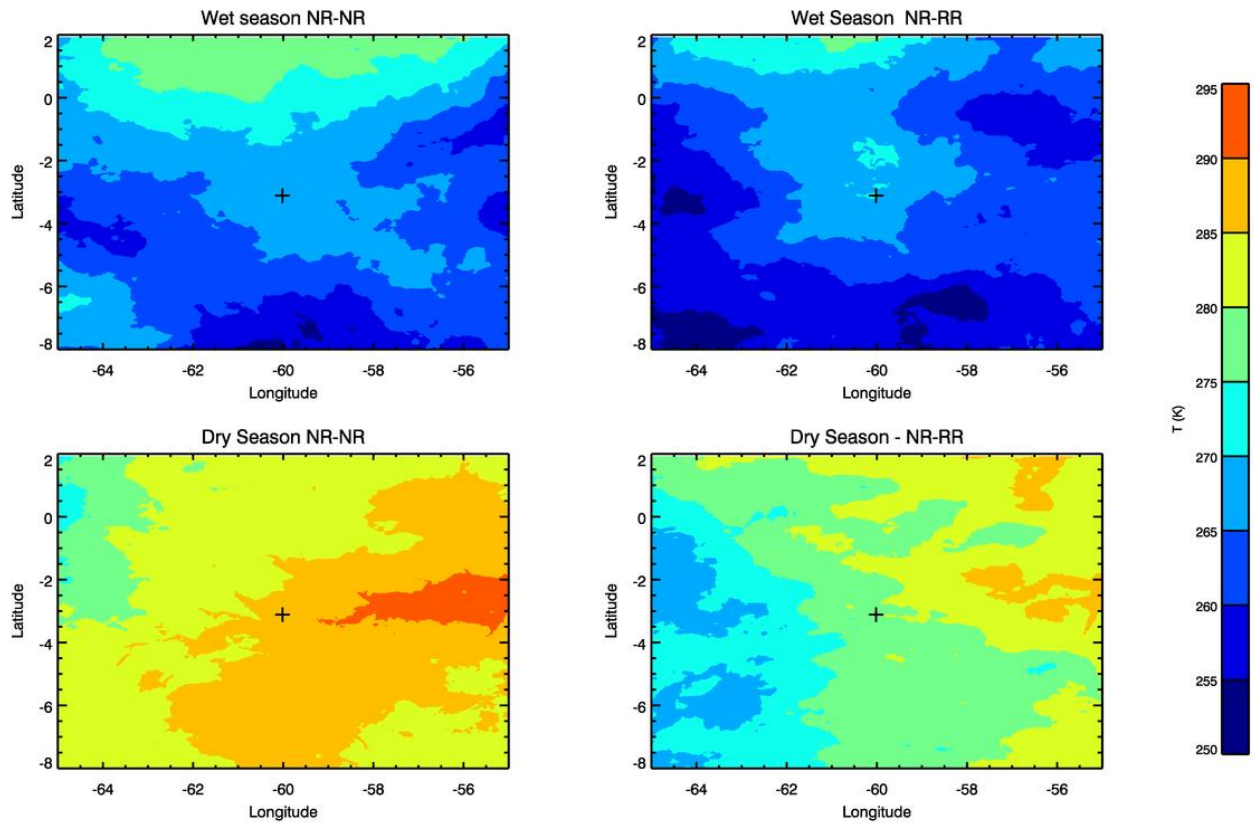


Figure 8: Mean GOES 10.4 μm brightness temperature fields from 2000 LT to 0800 LT, for dry and wet seasons and NR-NR and NR-RR transitions. The cross mark represents the T3 position.

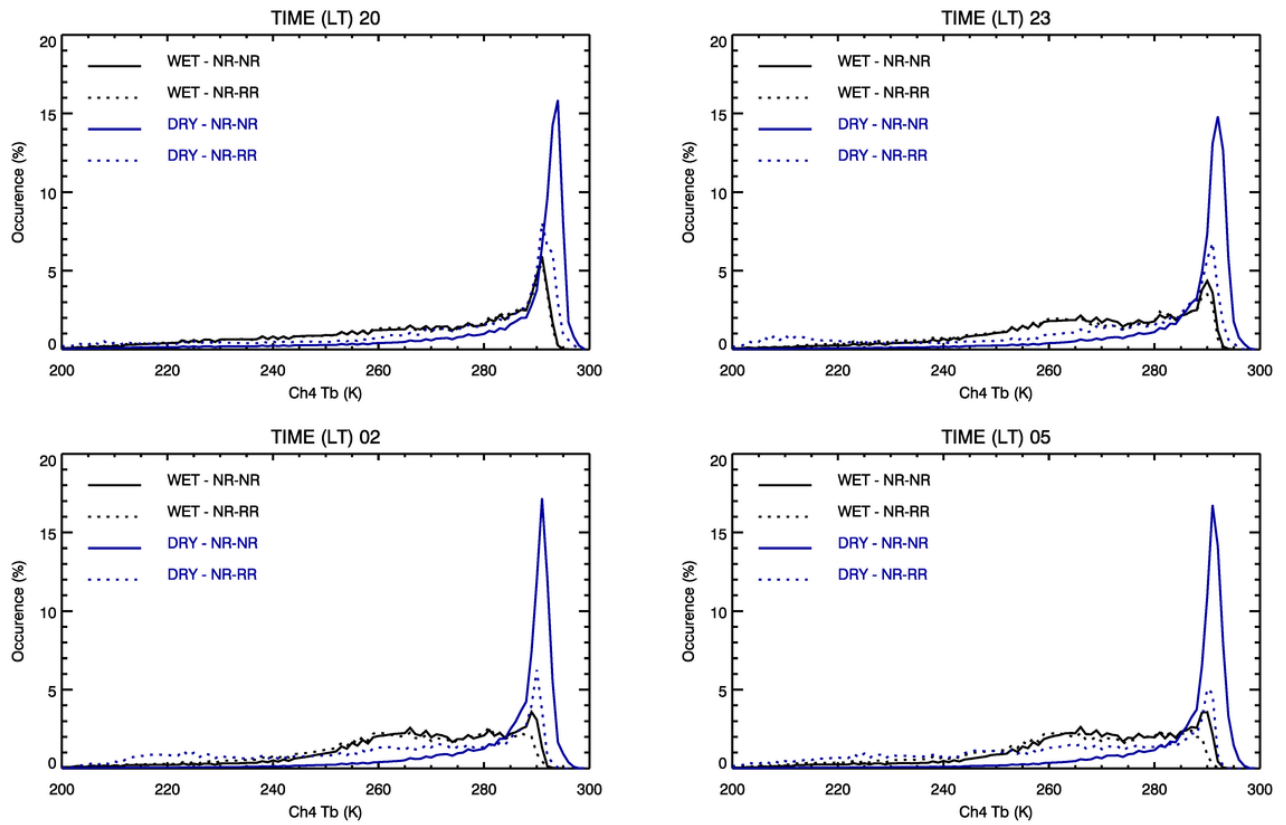


Figure 9: Probability distributions (grouped in 3h groups) of GOES 10.4 μm brightness temperatures, for the wet season and nocturnal period. Time at each panel is the start time (LT)

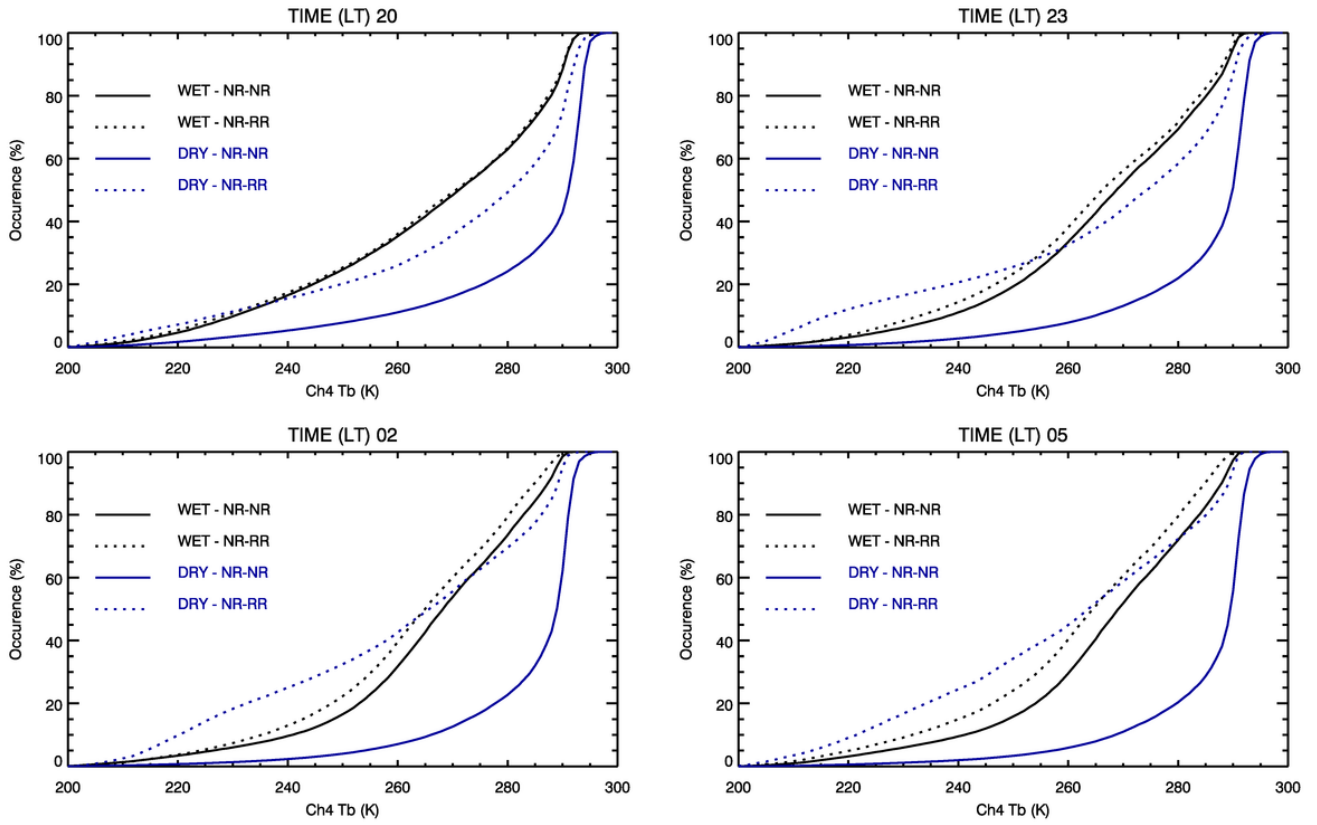


Figure 10: Cumulative distribution functions (grouped in 3h groups) of GOES 10.4 μm brightness temperatures, for the wet season and nocturnal period. Time at each panel is the start time (LT)